



A high-flux polyimide hollow fiber membrane to minimize footprint and energy penalty for CO₂ recovery from flue gas

Ryan P. Lively^{a,*}, Michelle E. Dose^{a,b}, Liren Xu^b, Justin T. Vaughn^b, J.R. Johnson^b, Joshua A. Thompson^b, Ke Zhang^b, Megan E. Lydon^c, Jong-Suk Lee^b, Lu Liu^b, Zushou Hu^b, Oğuz Karvan^b, Matthew J. Realff^b, William J. Koros^b

^a Algenol Biofuels, 28100 Bonita Grande Drive, Bonita Springs, FL 34315, USA

^b School of Chemical and Biomolecular Engineering, Georgia Institute of Technology, 311 Ferst Drive, Atlanta, GA 30332-0100, USA

^c School of Chemistry and Biochemistry, Georgia Institute of Technology, 901 Atlantic Drive, Atlanta, GA 30332-0400, USA

ARTICLE INFO

Article history:

Received 27 June 2012

Received in revised form

12 August 2012

Accepted 13 August 2012

Available online 24 August 2012

Keywords:

Hollow fiber membranes

Mixed matrix membranes

Zeolitic imidazolate frameworks

CO₂ capture

System footprint

ABSTRACT

Using a process-guided approach, a new 6FDA-based polyimide — 6FDA–DAM:DABA(4:1) — has been developed in the form of hollow fiber membranes for CO₂ recovery from post-combustion flue gas streams. Dense film studies on this polymer reveal a CO₂ permeability of 224 Barrers at 40 °C at a CO₂ feed pressure of 10 psia. The dense films exhibit an ideal CO₂/N₂ permselectivity of 20 at 40 °C, which permits their use in a two-step counter-flow/sweep membrane process. Dry-jet, wet-quench, non-solvent-induced phase inversion spinning was used to create defect-free hollow fibers from 6FDA–DAM:DABA(4:1). Membranes with defect-free skin layers, approximately 415 nm thick, were obtained with a pure CO₂ permeance of 520 GPU at 30 °C and an ideal CO₂/N₂ permselectivity of 24. Mixed gas permeation and wet gas permeation are presented for the fibers. The CO₂ permeance in the fibers was reduced by approximately a factor of 2 in feeds with 80% humidity. As a proof-of-concept path forward to increase CO₂ flux, we incorporated microporous ZIF-8 fillers into 6FDA–DAM:DABA(4:1) dense films. Our 6FDA–DAM:DABA(4:1)/ZIF-8 dense film composites (20 wt% ZIF-8) had a CO₂ permeability of 550 Barrers and a CO₂/N₂ selectivity of 19 at 35 °C. Good adhesion between the ZIF and the 6FDA–DAM:DABA(4:1) matrix was observed. CO₂ capture costs of \$27/ton of CO₂ using the current, “non-optimized” membrane are estimated using a custom counterflow membrane model. Hollow fiber membrane modules were estimated to have order-of-magnitude reductions in system footprint relative to spiral-wound modules, thereby making them attractive in current space-constrained coal-fired power stations.

© 2012 Elsevier B.V. All rights reserved.

1. Introduction

Despite the recent recession-induced downturn in worldwide CO₂ emissions, the US Energy Information Association predicts a steady increase in US CO₂ emissions over the next 25 years (approximately +0.025 gigatons (Gt) of CO₂/yr increase) [1]. Furthermore, developing countries are expected to drastically increase worldwide CO₂ emissions; a much sharper increase in worldwide emissions over the same time span is predicted (approximately +0.62 Gt CO₂/yr increase) [2]. Current global CO₂ emissions for 2012 are approximately 37.4 Gt CO₂/yr [2]. As many developed countries currently import products and commodities with high CO₂ intensities from developing countries, countries with strong foundations in science and

engineering should provide global, scalable solutions for reducing CO₂ emissions.

Over 3250 coal-fired power plants are installed throughout the world (1627 GW total capacity, with the average unit being 500 MW_e) [3]. These stable and reliable “base load” utilities are major drivers behind anthropogenic CO₂ emissions [4]. Unfortunately, reducing the CO₂ intensity of these plants is difficult due to: (i) massive coal and air intake rates requiring any separation system associated with such a plant to be “world-scale”, (ii) flue gases contain high concentrations of water, acid gases (SO_x, NO_x), oxygen and particulates, and (iii) are typically at low temperature and pressure. The massive scales require discussion of meaningful CO₂ abatement from coal-fired power plants to focus on the scalability of the separation device. To put the scale of the problem into perspective, some of the largest high-pressure natural gas processing plants in the US (9 total plants with > 1.2 billion scfd feed rate) [5], are only slightly larger than the low-pressure flue gas molar exhaust of *each* of the ~500 power plants

* Corresponding author. Tel.: +1 404 385 4717; fax: +1 404 385 2683.
E-mail address: ryan.lively@algenol.com (R.P. Lively).

in the US [4]. Here, we discuss a membrane solution that utilizes the proven scalability of the hollow fiber spinning platform to address post-combustion CO₂ capture at global scales, with a goal to control the required capture plant “real estate” as well as the energy penalty to perform the capture process.

Membrane-based single-stage post-combustion CO₂ capture appears unattractive unless ultra-high permeability and selectivities can be achieved [6]. On the other hand, multi-stage membrane processes with downstream vacuum (rather than upstream compression) lead to significant reductions in energy consumption and appear viable [7–9]. In particular, Membrane Technology Research (MTR) has developed a multi-stage membrane process utilizing the power station boiler feed air in a counter-flow sweep arrangement [10,11] to increase the CO₂ partial pressure in the combustion exhaust gas from the boiler. This approach increases the driving force for the subsequent CO₂ separation using three membrane stages. The first stage removes the majority of the CO₂ from the flue gas using a downstream vacuum with a pressure ratio across the membrane of approximately five [10]. The second stage is the aforementioned counter-flow sweep membrane which contacts the retentate gas from the first stage with boiler feed air. After the permeate from the first stage is compressed and the majority of the CO₂ liquefied, a third stage membrane is utilized to recover any remaining gas-phase CO₂. The permeate from the third stage is recycled to the feed of the third stage membrane, while the retentate is recycled to the feed of the first membrane. Utilizing the rubbery PolarisTM membrane in spiral-wound elements, MTR estimates the total cost of the process to be about \$23/ton of CO₂ using approximately 1.3 MM m² of membrane surface area (550 MW_e coal-fired power plant basis). A recent analysis by DOE-NETL using the counter-flow sweep arrangement predicts a CO₂ capture cost of approximately \$27–\$37/ton of CO₂, depending on the host plant [12]. We estimate that approximately 50,000 modules (20.3 cm inner diameter, 100 cm long, 600 m²/m³) will be required for each power plant using PolarisTM spiral-wound membrane modules.

While rubbery membranes have been primarily considered for post-combustion CO₂ capture [13–16], the difficulties associated with mass production of low-footprint, surface-area-efficient devices may preclude their wide-spread adoption, which is necessary to promote meaningful CO₂ emission reductions. On the other hand, 6FDA-based glassy polyimides have proven to be a tunable polymer family that are readily spinnable as hollow fiber membranes [17–19]. Hollow fiber membrane fabrication systems have exceedingly high production rates due to multi-filament spinning capabilities [20] and offer module surface area-to-volume ratios approaching 10,000 m²/m³. Typically, the thicker selective layers in hollow fiber membranes offset some of the surface area advantage of the fiber morphology [21], but an order of magnitude increase in module productivity per unit volume is feasible for the same base polymer. As noted by MTR and other researchers, for the case of post-combustion CO₂ capture, CO₂ flux through the membrane is the most paramount membrane characteristic to minimize required membrane area provided a satisfactory CO₂/N₂ selectivity can be achieved (> ~20) [10]. Previous work has argued that a minimum selectivity of 30 is required to capture advantages of the two-step counter-flow/sweep multi-stage process [10], but as we show here, the process is still viable with selectivities of at least 20.

With such a “high flux, moderately selective” framework in mind, we chose to develop a 6FDA dianhydride-based copolymer using constituent ratios of DAM and DABA diamines that would achieve this goal. 6FDA–DAM constituents tend to promote high CO₂ permeability, yet low CO₂/N₂ selectivity, and 6FDA–DABA constituents promote high selectivity, yet low permeability. Previous work using 6FDA–DAM:DABA(2:1) and 6FDA–DAM [22,23] suggest that the former is “too selective” (> 30) and “too slow” while the latter

was found to be sufficiently permeable, but not selective enough (< 17) for low-cost CO₂ capture. Here, we synthesize and characterize 6FDA–DAM:DABA(4:1) dense films and hollow fiber membranes to find the appropriate middle ground between the two previously studied 6FDA-based copolymers.

Finally, we explore a “proof-of-concept” route to boost the permeability of 6FDA–DAM:DABA(4:1) by utilizing a mixed matrix membrane approach. Here, we utilize the commercially available zeolitic imidazolate framework (ZIF) “ZIF-8” as a permeability-enhancing filler. ZIF-8 has been shown to be: (i) highly hydrophobic [24], justifying its use over mesoporous fillers (which would “wet out” at high feed gas water activities), (ii) highly permeable to CO₂ with moderate CO₂/N₂ selectivities [25], and (iii) due to its organic nature, easily adherent to the host polymer matrix [25,26]. While other fillers may enhance selectivity and permeability (such as zeolites), there are very few — if any — sufficiently small fillers that can be readily incorporated into the polymer matrix without surface modification and can also withstand high water activities typically found in combustion flue gases. The choice of the 6FDA–DAM:DABA(4:1) and ZIF-8 pair is a good choice as a proof-of-concept for downsizing CO₂ capture plant footprints while maintaining reasonably low parasitic load to operate the CO₂ capture process.

2. Background/experimental

2.1. Materials

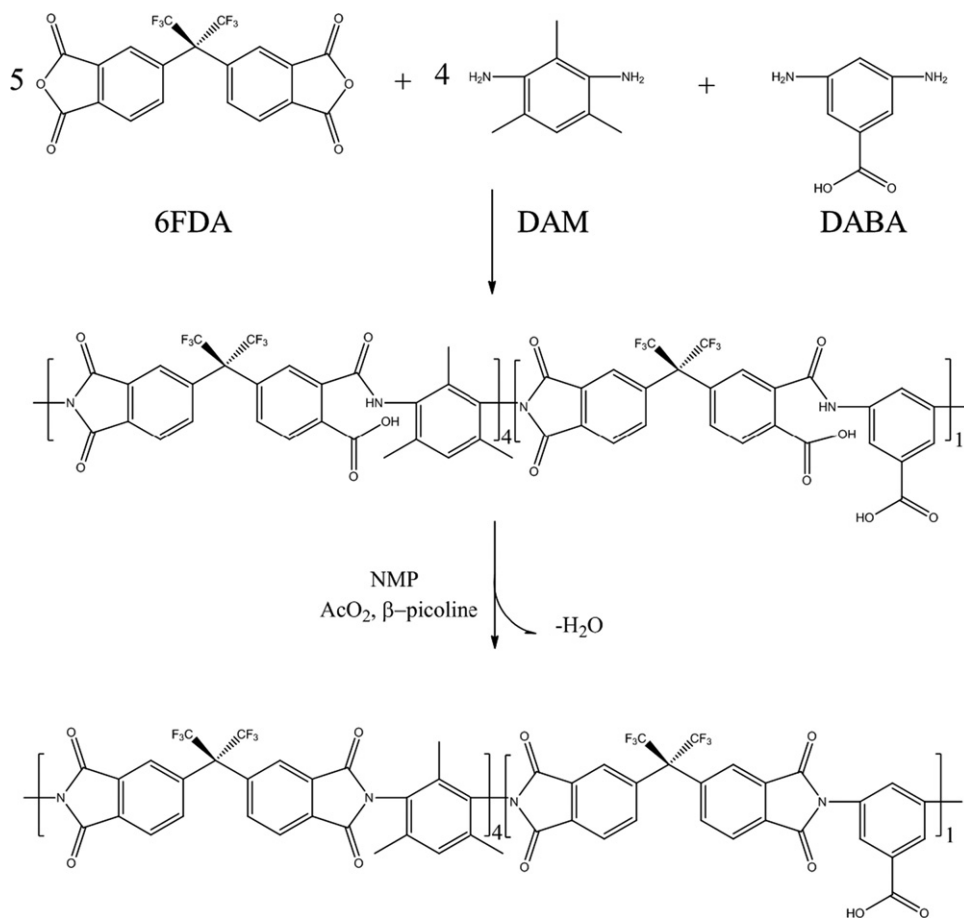
4,4'-Hexafluoroisopropylidene diphthalic anhydride (6FDA) was purchased from Alfa Aesar, and dried at 150 °C under 30 mm Hg reduced pressure. 2,4,6-Trimethyl-1,3-diaminobenzene (DAM) and 3,5-diaminobenzoic acid (DABA) were dried at 60 °C and 150 °C, respectively, under 30 mm Hg reduced pressure. N-methyl pyrrolidone (NMP), acetic anhydride (AcO₂) and beta picoline (3-methyl pyridine) were dried over activated 5A molecular sieves prior to the synthesis. All chemicals, besides 6FDA, were purchased from Sigma Aldrich (Milwaukee, WI). All glassware was flamed with a propane torch and N₂ purge prior to the reaction. Anhydrous tetrahydrofuran (THF), ethanol, dichloromethane (DCM), lithium nitrate, and ZIF-8 were all purchased from Sigma-Aldrich. Polydimethylsiloxane (PDMS, Sylgard 184) was obtained from Dow Chemicals.

2.2. 6FDA–DAM:DABA (4:1) synthesis

6FDA–DAM:DABA(4:1) was synthesized through a one-pot, two-step reaction sequence [19]. In the first step, 6FDA dianhydride was reacted with DAM and DABA diamines under flowing N₂ in a 5:4 (6FDA:DAM) and 5:1 (6FDA:DABA) molar ratio (Scheme 1). The total solid concentration was 20 wt% in NMP. The reaction temperature was kept between 0 °C and 5 °C and diamines were added incrementally over a period of ~2 h. Slow addition and low temperatures are necessary for the formation of high molecular weight polymers. The reaction was run for 24 h, during which time the temperature slowly rose back to room temperature. The resulting polyamic acid was closed through chemical imidization, whereby beta picoline and acetic anhydride were added and stirred for an additional 24 h under flowing N₂ at room temperature. The resulting polyimide was precipitated and washed in MeOH, followed by drying under vacuum at 210 °C for 24 h.

2.3. Film casting

Pure 6FDA–DAM:DABA(4:1) dense films were made from 6FDA–DAM:DABA(4:1)-dichloromethane solutions. The polymer



Scheme 1. Synthesis of 6FDA–DAM:DABA(4:1).

solution was allowed to mix on a coaxial roller for 24 h prior to use. Dense films were prepared by pouring a portion of the solution on to an untreated glass plate and casting with a 10 mil casting knife in a N_2 filled, DCM-saturated glove bag. After 18–24 h in the glove bag, the film was removed from the plate and transferred to a vacuum oven at 200 °C and held at that temperature for 24 h. After naturally cooling to room temperature under vacuum, the films were mounted for permeation testing.

Preparation of 20 wt% ZIF-8/6FDA–DAM:DABA(4:1) mixed matrix membranes was more complex. Approximately 0.75 g of vacuum-dried ZIF-8 was added to 27 g of DCM. The ZIF-8/DCM mixture was then homogenized with three 60 s bursts from a sonication horn (1000 W max. horn, Dukane, Leesburg, VA) with 90 s of vigorous vortex mixing (Digital Vortex Mixer 120 V, Fisher Scientific) between bursts. Initially, 10% of the total polymer was added to the ZIF-8/DCM dispersion, using two 60 s bursts of sonication to homogenize the dispersion/solution. This step accelerated an unknown undesirable reaction between the ZIF-8 and the polymer, causing the mixture to form a solid gel that was impossible to properly cast. To avoid this phenomenon, this sonication step was omitted and the polymer was added as described: immediately following the last sonication treatment to the ZIF-8/DCM dispersion, 3.0 g of polymer was slowly added to the mixture, using vortex mixing to dissolve the polymer after each addition. After all the polymer was dissolved, the ZIF-8/DCM/6FDA–DAM:DABA(4:1) mixture was immediately cast in the same manner as the pure polymer films. Sonication of ZIF-8 in the presence of the polymer was avoided. The same drying and annealing procedures for the pure polymer film were followed. In addition, a sample of the “gelled” ZIF-8/DCM/6FDA–DAM:DABA(4:1) was made for X-ray diffraction analysis.

2.4. Materials characterization

Glass transition temperatures for neat 6FDA–DAM:DABA(4:1) and its corresponding mixed matrix membranes were measured by using differential scanning calorimetry (DSC, model TA Instruments Q200). Each run was made from 0 °C to 420 °C at a heating rate of 10 °C/min. The T_g was determined from the second DSC sweep. Thermogravimetric analysis (TGA, Netzch STA 409 PC TGA Burlington, MA) was used to determine the degradation temperatures of the membranes. Samples were heated to a temperature of 600 °C under a nitrogen purge at a ramp rate of 10 °C/min. Powder X-ray diffraction (XRD) was performed at room temperature on an X’Pert Pro PANalytical X-ray Diffractometer using Cu-K α radiation. Measurements were carried out from 5–40° 2θ , using an X’celerator detector with low-background sample holders. Attenuated total reflectance spectroscopy (ATR) was performed using a Bruker Vertex 80v FTIR spectrometer coupled to a Hyperion 2000 IR microscope containing a 20x magnification ATR objective with a Germanium crystal.

2.5. Permeation

Gas permeation through an asymmetric hollow fiber membrane and a dense film is typically described using the solution-diffusion theory, and the permeability (“productivity”) of the polymer can be expressed as shown in Eq. (1)

$$P_i = D_i S_i \quad (1)$$

where P_i typically has units of Barrers [$10^{-10} \text{ cm}^3(\text{STP})\text{-cm/cm}^2\text{-s-cm Hg}$], D_i [cm^2/s] is defined as the transport diffusivity of

component i through the membrane and S_i [$\text{cm}^3(\text{STP})/\text{cm}^3$ polymer-cm Hg] is the solubility coefficient of component i in the membrane. Permeability is further defined as the flux of component i normalized by the transmembrane pressure Δp [atm] and the film thickness l [cm], viz.,

$$P_i = \frac{(\text{flux})_i \ell}{\Delta p_i} \quad (2)$$

The ratio of the permeability of component i and component j — the ideal permselectivity (“efficiency”) of the membrane — is given by:

$$\alpha_{ij} = \frac{P_i}{P_j} \quad (3)$$

and can be broken into the diffusion selectivity and the solubility selectivity, viz. [27],

$$\frac{P_i}{P_j} = \left(\frac{D_i}{D_j}\right) \left(\frac{S_i}{S_j}\right) \quad (4)$$

Permeation through a membrane occurs via an activated process, and exhibits an apparent Arrhenius dependence on temperature, viz.,

$$P_i = P_{i,0} \exp\left(\frac{-E_{p,i}}{RT}\right) \quad (5)$$

where $P_{i,0}$ [Barrers] is the exponential pre-factor, and E_p [kJ/mol] is the activation energy of permeation. In situations where the skin thickness is difficult to determine (i.e., asymmetric membranes), the “permeance,” defined as the partial pressure difference normalized flux is given by:

$$\left(\frac{P}{\ell}\right)_i = \frac{(\text{flux})_i}{\Delta p_i} \quad (6)$$

Permeation tests on the dense 6FDA–DAM:DABA(4:1) films were performed using an isochoric system [27,28], where measurements of the film’s thickness, permeable surface area, feed pressure, and the rise of pressure in the downstream of the system (which is proportional to the molar flow rate through the film) permit the calculation of the intrinsic permeability of the polymer. Care was taken to test N_2 first, followed by CO_2 , and then N_2 was re-tested to confirm the polymer did not undergo permanent CO_2 -induced changes. Measurements were repeated three times on the same film, and a second film was cast and made to verify the values of the first film. Here, the error bars represent one standard deviation from the average of all the permeation experiments.

6FDA–DAM:DABA(4:1) hollow fibers were assembled into 20 cm long shell-and-tube modules with 5–6 fibers each [27]. The permeance of the fibers was tested using pure gas measurements in a constant pressure system, and multiple modules from each spin state were tested. Feed pressures of 20 psia were used to simulate flue gas conditions. After testing, the fibers were post-treated (if necessary) with a 3 wt% high molecular weight polydimethylsiloxane solution in heptane to seal any pinhole defects in the selective skin layer [29]. Mixed gas measurements were performed using a mixture of CO_2/N_2 (20 mol% CO_2) which was fed to the fibers on the shell side at 30 °C–50 °C. A feed pressure of 100 psia was used to generate sufficient permeate for sampling. The retentate flow rate was set such that the stage cut across the fiber was less than 3% [30]. The permeate flow rate was measured with a bubble flow meter and its composition was analyzed via gas chromatography.

Wet gas measurements on the hollow fiber membranes were made by saturating pure CO_2 or pure N_2 with a custom-built gas saturating system (Supplementary information). This system utilizes a water evaporator (Controlled Evaporator Mixer,

Bronkhorst USA Inc., Bethelhem, PA) that mixes water vapor with the pure gas feed using mass flow controllers. The humidity of the feed gas was set to 80% R.H., which was the maximum the saturating system could provide stably. The wet feed gas was supplied to the shell side of the fibers, and a needle valve set the retentate flow rate to 740 mL/min at a 20 psia feed pressure. The permeate humidity was monitored, and the permeate flow rate was measured using a bubble flow meter. Knowledge of the permeate humidity and feed humidity allowed for calculation of the gas permeance.

2.6. Sorption

Gas sorption coefficients in polymeric materials exhibit van’t Hoff temperature dependencies, viz.,

$$S_i = S_{i,0} \exp\left(\frac{-H_{S,i}}{RT}\right) \quad (7)$$

where $S_{i,0}$ [$\text{cm}^3(\text{STP})/\text{cm}^3$ polymer-cm Hg] is the exponential pre-factor, and H_S [kJ/mol] is the apparent heat of sorption into the polymer (this term combines the heat of sorption into the unrelaxed volume of the polymer and into the “dissolved” states [31]). The heat of sorption can be used as a gauge of the interaction between the gas penetrant and the polymer; more negative values indicate stronger attractions between the pair. CO_2 and N_2 sorption isotherms in 6FDA–DAM:DABA(4:1) were obtained using the piezometric method known as “pressure decay” sorption [32].

The vapor adsorption equilibria on 6FDA–DAM:DABA(4:1), ZIF-8 and the 20 wt% ZIF-8/6FDA–DAM:DABA(4:1) mixed matrix membrane were obtained using a VTI-SA vapor sorption analyzer from TA Instruments (New Castle, DE, United States) at a temperature of 30 °C. The vapor activity was controlled automatically by mixing the wet vapor feed with a dry N_2 line. As such, N_2 serves as a carrier gas for the vapors. The sample’s “dry mass” was measured under N_2 and were at equilibrium with N_2 before introduction of the vapors to the sample chamber.

2.7. Hollow fiber spinning

6FDA–DAM:DABA(4:1) fibers were produced via dry-jet, wet-quench, non-solvent-induced phase separation spinning. 6FDA–DAM:DABA(4:1) dopes were based on dopes capable of making defect-free skin layers for a similar polymer, 6FDA–DAM:DABA(3:2) [18]. The synthesized polymer was dried at 110 °C under vacuum overnight prior to its addition to the solvent/non-solvent solution. The dope composition and spinning conditions can be found in Table 1 [19]. The polymer solution was stirred for a week in a sealed container at 45 °C until a clear, viscous solution was observed. After degassing, the dopes were loaded into 500 mL ISCO pumps (Model 500D, Teledyne ISCO, Inc., Lincoln NE). The fibers were extruded through a co-annular die (“spinneret”) into a 50 °C, 2 m traversal length water bath and were taken up at 50 m/min by a take-up drum. The fibers were taken off the drum by a clean razor cut and were subsequently soaked in deionized water for 3 days, with the water being changed every day. After the water soak, the fibers were soaked in methanol for an hour with the methanol being changed every 20 min. The same process was repeated using hexane as the final non-solvent rinse. Finally, the fibers were allowed to air dry for one day, and then put into a vacuum oven at 110 °C for 1 h.

2.8. Electron microscopy

Scanning electron microscopy (SEM) images were obtained using a LEO 1550 microscope. Fibers were fractured by first

Table 1
6FDA–DAM:DABA(4:1) hollow fiber dope formulation and spinning conditions.

Dope formulation		Spinning conditions	
Polymer	25.0 wt%	Dope extrusion rate	180 mL h ⁻¹
NMP	31.5 wt%	Bore fluid	60 mL h ⁻¹ , 80 wt%/20 wt% NMP/H ₂ O
THF	10.0 wt%	Bath temperature	50 °C
LiNO ₃	6.5 wt%	Spinneret temperature	70 °C
Ethanol	27.0 wt%	Air gap	2–16 cm
		Quench bath	Tap water, 2 m traversal length
		Take-up rate	50 m min ⁻¹

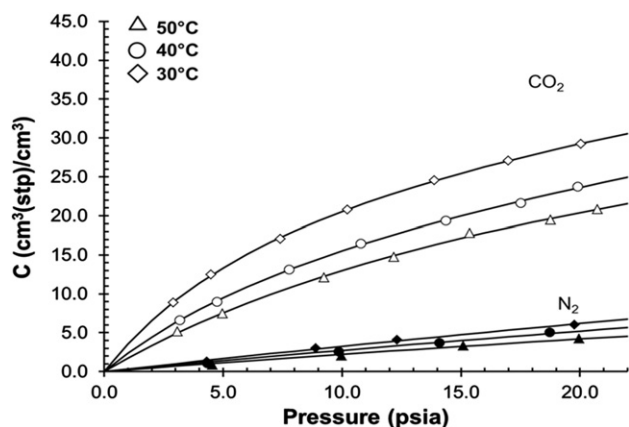


Fig. 1. CO₂ and N₂ pure gas sorption isotherms at 30 °C, 40 °C, and 50 °C on 6FDA–DAM:DABA(4:1) films annealed at 200 °C.

submerging short segments of fiber in hexane, and then cryogenically broken using tweezers under liquid nitrogen [33]. The fiber fragments were sputter coated with a 10–20 nm gold layer (Model P-S1 Sputter Coater, ISI, Mountain View CA). For transmission electron microscopy (TEM) imaging, ZIF-8/6FDA–DAM:DABA (4:1) membranes were embedded in epoxy and microtomed [34] using a 35° Diatome Diamond Knife and a Leica microtome. Epoxy slices were floated in water, and then adsorbed to a carbon-formvar-coated copper grid. Samples were dried at 80 °C overnight to remove water and dried in a vacuum chamber overnight prior to imaging. Bright field TEM images were obtained with a JEOL 400EX high resolution TEM (HRTEM) at 380 kV using a CCD camera and micrograph software.

3. Results and discussion

3.1. Neat polymer

3.1.1. Polymer synthesis

As shown in Fig. S1, ATR confirms near-complete imidization of 6FDA–DAM:DABA(4:1). DSC and TGA results (Figs. S2 and S3, respectively), reveal the polymer has a glass transition temperature of 380 °C — consistent with other 6FDA-based polyimides [19,22] — and a decomposition temperature of ~450 °C. Using gel permeation chromatography, the polymer was found to have a molecular weight of 80,200 g/mol with a polydispersity index of 2.35.

3.1.2. Sorption

Fig. 1 shows the CO₂ and N₂ sorption isotherms for 6FDA–DAM:DABA(4:1) at temperatures and pressures relevant to typical post-combustion flue gases. The solubility coefficient for gas sorption into the 6FDA–DAM:DABA(4:1) was determined by

Table 2

Sorption and transport properties of 6FDA–DAM:DABA(4:1) at low pressures (< 20 psia).

T (°C)	D _{CO₂} [cm ² /s]	D _{CO₂} /D _{N₂}	S _{CO₂} /S _{N₂}	P _{CO₂} (10 psia) [Barrers]	P _{CO₂} /P _{N₂}
30	5.4 × 10 ⁻⁸	3.4	6.2	211.4 ± 0.3	21.3
40	7.5 × 10 ⁻⁸	3.3	5.7	224.1 ± 0.5	20.4
50	9.7 × 10 ⁻⁸	3.2	5.9	242.9 ± 2	19.4

on the secant slope of the sorption isotherms (between 10 psia and 0 psia). As shown in Table 2, the CO₂/N₂ solubility selectivity in 6FDA–DAM:DABA(4:1) is approximately 6 for the temperatures investigated here. The heat of sorption (Table 3) for CO₂ was found to be -28.3 ± 1.2 kJ/mol, while N₂ was found to have a value of -22.7 ± 1.4 kJ/mol, indicating that the solubility selectivity will decrease with increasing temperature, as expected [31]. Furthermore, the heat of sorption is more negative than other 6FDA-based polymers [31], implying a stronger attraction between the CO₂ and the polymer matrix, either as a result of the free carboxylic acid in the polymer backbone or a more open structure than other 6FDA-based polyimides with temperature-dependent data published. From a solubility perspective alone, operating the post-combustion membrane unit at lower temperatures will result in the most favorable selectivities.

3.1.3. Dense film permeation

The CO₂/N₂ permeability and permselectivity at temperatures and pressures relevant to post-combustion CO₂ capture are shown in Table 2. The diffusion coefficient was calculated from Eq. (1) using the solubility coefficient from the sorption isotherms and the permeability from the dense film permeation experiments. We investigated feed pressures from 5 psia to 20 psia and did not observe any noteworthy pressure-dependent changes in permeability and permselectivity.

The CO₂ permeability in 6FDA–DAM:DABA(4:1) is high for a glassy polymer, and exists between 6FDA–DAM [22] and 6FDA–DAM:DABA(2:1) [21], as expected. 6FDA–DAM:DABA(4:1) sits below the 2008 polymer upper bound. The polymer upper bound for CO₂/N₂ separations is dominated by rubbery polymers [35], primarily due to their high solubility selectivities and high CO₂ permeabilities. As shown in Table 3, the activation energy of permeability of CO₂ was found to be lower than that of N₂ by nearly 35%, and was also positive, indicating that permeability will increase with increasing temperature. This indicates that while diffusion and sorption have competing temperature-dependent contributions to the permeability of a gas penetrant, the temperature dependence of the diffusion contribution is the dominating factor. As the difference in the activation energy of permeation between CO₂ and N₂ is negative, a decrease in permselectivity is expected with an increase in temperature [31].

The diffusion coefficient was found to almost double between 30 °C and 50 °C, and the diffusivity selectivity was found to be

Table 3
Temperature dependent properties of 6FDA–DAM:DABA(4:1) films and fibers and 30 °C CO₂/N₂ permselectivities.

Film	Film			Fiber		
	E_p (kJ/mol) (200 °C annealed)	H_s (kJ/mol)	E_d (kJ/mol)	α_{CO_2/N_2}	E_p (kJ/mol) (110 °C annealed)	α_{CO_2/N_2}
CO ₂	6.2 ± 0.5	−28.3 ± 1.2	34.5 ± 1.7	20.8	8.2 ± 1.2	23.5
N ₂	9.63 ± 0.8	−22.7 ± 1.4	32.3 ± 2.2		11.1 ± 0.7	

approximately 3.3 for all temperatures studied. The temperature dependence of diffusion can be defined, viz.,

$$D_i = D_{i,0} \exp\left(\frac{-E_{D,i}}{RT}\right) \quad (8)$$

and is found by taking the difference between the activation energy of permeation and the heat of sorption [31]. Here, $D_{i,0}$ [cm²/s] is the pre-factor, and $E_{D,i}$ [kJ/mol] is the activation energy of diffusion. The activation energies of diffusion for both CO₂ and N₂ in 6FDA–DAM:DABA(4:1) were found to be similar. This is an interesting observation especially in light of previous work which shows that E_{D,N_2} for non-DABA-containing polyimides is typically much higher than E_{D,CO_2} , reflecting the larger size of N₂ [28].

Taken as a whole, it appears that the primary driver for the CO₂/N₂ separation within 6FDA–DAM:DABA(4:1) is the solubility selectivity, rather than the diffusion selectivity, with the solubility selectivity being approximately 2/3rd of the total selectivity. This is contrary to results on other polyimides for other gas pairs such as O₂/N₂, where the diffusion selectivity greatly dominates the solubility selectivity [36]. However, the diffusion selectivity still plays an important role in the overall selectivity of the polymer. The solubility selectivity and the similar activation energies of diffusion likely derives in part from the pendant carboxylic acid on the DABA group, which exerts both a hydrogen bonding force and an induced dipole interaction with both the quadrupoles and lone pairs of CO₂ [37]. Nitrogen's weak quadrupoles and lower critical temperature reduce its interaction (relative to CO₂) with the pendant carboxylic acid group on the DABA constituent of the 6FDA–DAM:DABA(4:1) polymer matrix. Carbon dioxide's interaction with the carboxylic acid will become weaker at higher temperatures, which will decrease the solubility of CO₂ in the polymer matrix (along with a corresponding increase in polymer segmental chain mobility) which will decrease the overall selectivity of the polymer. The more condensable nature of CO₂ relative to N₂ will also aid the solubility selectivity. With the goal of maintaining a selectivity of at least 20 with a CO₂ permeability as high as possible, these experiments reveal that an operating temperature of approximately 40 °C is appropriate, and is close to typical post-flue gas desulfurization (FGD) temperatures [38].

3.1.4. Hollow fiber spinning and permeation

3.1.4.1. Air gap and skin layer formation. By utilizing an optimized spinning procedure developed for 6FDA–DAM:DABA(3:2) [18], we were able to spin defect-free 6FDA–DAM:DABA(4:1) hollow fibers by varying the air gap from 2 cm to 16 cm. The resulting fibers were approximately 257 μm OD and 130 μm ID. Fibers spun using an air gap of 2 cm (0.024 s air gap residence time) were found to be defect-free. As shown in Fig. 2, as the residence time in the air gap increased, we observed a decrease in the ideal CO₂/N₂ permselectivity in the hollow fiber sorbents. As the air gap height increases, we hypothesize that the increased residence time in the air gap results in greater moisture absorption into the

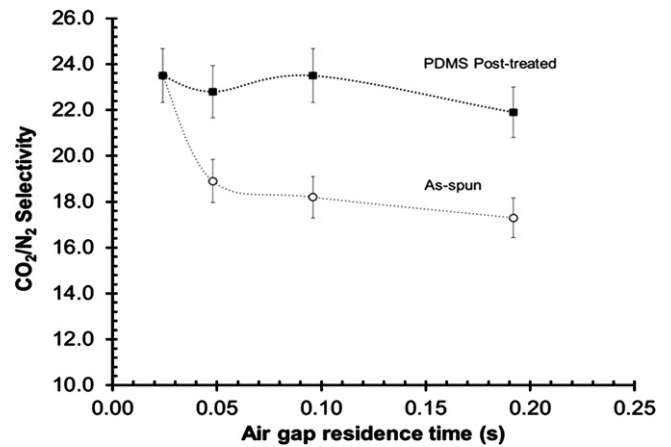


Fig. 2. Ideal CO₂/N₂ permselectivities of 6FDA–DAM:DABA(4:1) hollow fiber membranes at 30 °C as a function of nascent fiber residence time in the air gap. Open circles are the as-spun hollow fibers, whereas the black squares are the PDMS post-treated fibers. The dotted lines serve as a guide for the eye. Error bars represent one standard deviation away from the average of multiple modules.

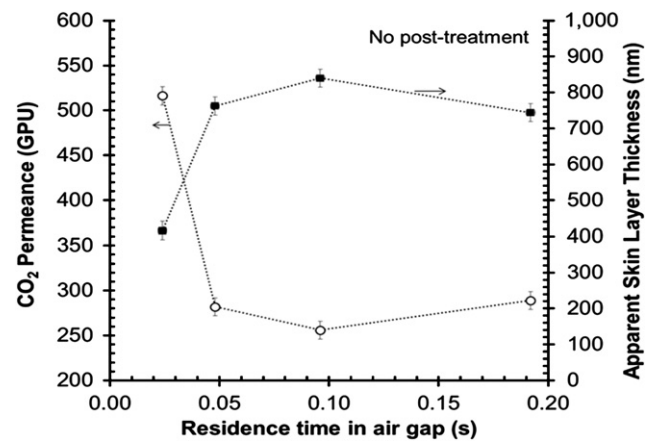


Fig. 3. CO₂ permeance (open circles) and apparent skin layer thickness (black squares) of 6FDA–DAM:DABA(4:1) hollow fiber membranes. The dotted lines serve as a guide for the eye. Error bars represent one standard deviation away from the average of multiple modules. 1 GPU = 10^{−6} cm³(STP)/cm²·s·cm Hg.

nascent fiber, leading to interfacial phase separation in the air gap. However, all of the states were “repairable” with a standard PDMS post-treatment (Fig. 2) [29]. Defect-free fibers are desirable, making the PDMS post-treatment step unnecessary, which may reduce module production costs.

The apparent skin layer thickness of the asymmetric fiber can be estimated, viz.,

$$\ell = \frac{(\text{Permeability})_i}{(\text{Permeance})_i} \quad (9)$$

As shown in Fig. 3, the skin layer thickness appears to asymptote at approximately 800 nm as the residence time in the air gap continues to increase. This is expected assuming Fickian diffusion and subsequent evaporation of volatile solvents and non-solvents out of the nascent fiber skin layer. The evaporation of the solvent and non-solvent essentially dictates the skin layer thickness of the nascent asymmetric membrane. If a constant solvent diffusion coefficient through the dense skin layer is assumed, the evaporation rate of the solvent and non-solvent will decrease with the square of the skin layer's increasing thickness, thus essentially “self-limiting” the growth of the skin layer, assuming temperature, relative humidity and air convection rate

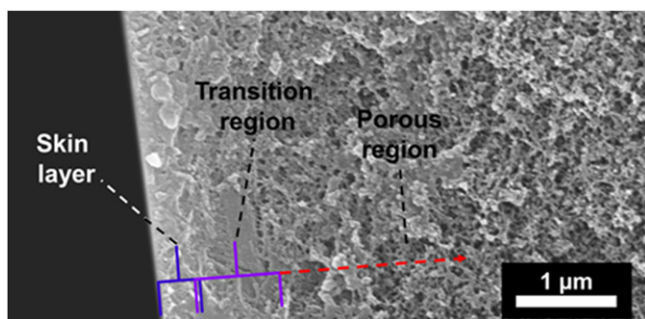


Fig. 4. Representative SEM micrograph of defect-free 6FDA–DAM:DABA(4:1) hollow fiber membrane skin.

around the wet-jet are held constant and that the fiber undergoes spinodal decomposition in the quench bath. A representative SEM image of the defect-free 6FDA–DAM:DABA(4:1) skin layer is shown in Fig. 4. A skin layer of approximately 400 nm is visible, as well as a transition region and the porous support beneath the skin.

3.1.4.2. Hollow fiber permeance and activation energy of permeation

The pure CO₂ permeance of the defect-free asymmetric hollow fiber membranes was found to be approximately 520 ± 9 GPU [1 GPU = 10^{-6} cm³(STP)/cm²·s·cm Hg], which is quite high and within a factor of two of the Polaris™ membrane (1000 GPU) [10]. As shown in Fig. 3, the CO₂ permeance asymptotically decreases with an increase in the air gap residence time, essentially leveling off at approximately 290 ± 5 GPU. We varied the temperature of the permeation experiment to compare the activation energy of permeation between the dense film and the hollow fibers. Table 3 shows the activation energy of the defect-free asymmetric hollow fibers, the dense films, and the CO₂/N₂ permselectivities of the two 6FDA–DAM:DABA(4:1) morphologies at 30 °C. The ideal selectivity of the hollow fiber membranes was found to be higher than the dense film results. This phenomenon has been seen before in 6FDA-based polymer spinning [17]. One hypothesis is that the extremely high shear rates in the spinneret (~ 2000 – $20,000$ s⁻¹) [39] combined with the rapid take-up rates results in uniaxial orientation of the polyimide polymer chains. This “oriented” arrangement presumably results in tighter packing of the polymer chains, which leads to an increase in gas permselectivity over the un-aligned state, but likely results in slower gas permeation through the selective layer [17]. The resulting activation energies of permeation for the hollow fibers were found to be higher than the dense films. This implies that the “activated state” required for permeation is more difficult to achieve in the fiber than in the dense films, lending support to the chain alignment hypothesis. Nonetheless, at 40 °C, defect-free fibers with pure CO₂ permeances of approximately 560 ± 6 GPU and a pure gas CO₂/N₂ permselectivities of approximately 21.0 were achieved. However, as the skin layers are still approximately 415 ± 10 nm thick, continued optimization of the spin dope and spinning conditions is required to reduce the skin thickness even further.

3.1.4.3. Mixed gas and wet gas permeation. Permeation measurements on the defect-free 6FDA–DAM:DABA(4:1) hollow fibers (air gap residence time of 0.024 s) were performed using 20 mol% CO₂/80 mol% N₂ feed gas to simulate the CO₂-enriched flue gas found in the two-step counter-flow/sweep arrangement considered here. Table 4 shows the mixed gas CO₂ permeance, mixed gas CO₂/N₂ permselectivity, CO₂ permeance in the presence of water and the CO₂/N₂ permselectivity in the presence of water.

Table 4
Mixed gas and wet gas permeances and permselectivities for defect-free 6FDA–DAM:DABA(4:1) hollow fiber membranes.

Mixed gas (20% CO ₂)	P_{CO_2} (GPUs)	$P_{\text{CO}_2}/P_{\text{N}_2}$
30 °C	320 ± 5	19.7
40 °C	381 ± 4	17.3
50 °C	400 ± 5	15.2
Wet gas (80% R.H.)		
30 °C	243 ± 2	20.9

Both the CO₂ permeance and permselectivity were found to be lower than the pure gas experiments, likely indicating competitive sorption effects favoring nitrogen. In mixed gas, the feed gas temperature strongly affects the permselectivity of the hollow fiber membrane. An increase in temperature from 30 °C to 50 °C reduces the permselectivity by 22% with an increase in permeance of approximately 20%. While an increase in permeance has been shown to be advantageous for low-cost post-combustion CO₂ capture [10], maintaining a selectivity of at least 20 is desirable to keep the membrane costs from escalating dramatically.

6FDA–DAM:DABA(4:1) hollow fiber membranes with wet CO₂ feeds (80% RH) were found to have significantly reduced CO₂ permeances relative to dry CO₂ feeds. This is likely due to strong water sorption in the unrelaxed volume of the glassy 6FDA–DAM:DABA(4:1), which leads to a decrease in CO₂ sorption in the polymer [40]. The decrease in CO₂ permeance could also be due to capillary condensation of water in the nano-pores in the transition layer sub-structure of the asymmetric hollow fiber membrane. The CO₂/N₂ permselectivity is slightly lower than that found in the pure gas experiments, presumably due to water out-competing the permanent gases for sorption sites, which would likely affect CO₂ more than N₂. While the loss of CO₂ permeance due to water is important, it is not a “show-stopper” as it is in other high fractional free volume polymers, where the CO₂ flux can be even more substantially retarded due to the presence of water [41]. Furthermore, the “wet CO₂” permeance of the 6FDA–DAM:DABA(4:1) hollow fibers is still high relative to other polymers being considered, and continuing efforts to reduce the skin layer thickness to approximately 100 nm from 415 nm will result in permeances similar to MTR’s Polaris™ membrane (~ 1000 GPUs) [10], even in wet feeds.

3.2. ZIF-8/6FDA–DAM:DABA(4:1) mixed matrix membranes

3.2.1. Dope preparation

During the mixed matrix membrane dope preparation, it was discovered that excessive thermal energy input led to the formation of a non-flowing, insoluble gel. While ZIF-8 has demonstrated thermal stability and stability to basic solutions [42], it is known that the ZIF is susceptible to even weak acids [43]. We hypothesize here that the pendant carboxylic acid on the solvated 6FDA–DAM:DABA(4:1) chains de-stabilize the exterior of the metal-imidazole framework and these pendant moieties subsequently crosslink to the ZIF particles. By minimizing the thermal energy input to the mixed matrix membrane dopes, this crosslinking was avoided, thus enabling film casting.

XRD was used to compare the ZIF-8 powder sample and the mixed-matrix membrane (MMM) samples. Fig. 5 shows the XRD patterns of the BASF ZIF-8 (a) with the typical *I*-43m cubic structure [44]. The composite film prepared at 20 wt% loading before the polymer dope seized into an insoluble gel (b) is shown in Fig. 5. The crystalline structure is maintained, and the broad,

amorphous peak associated with the 6FDA–DAM:DABA(4:1) polymer matrix can be seen. A dope of 20 wt% ZIF-8/6FDA–DAM:DABA(4:1) was intentionally gelled with sonication and dried in a vacuum oven. Powder XRD patterns of the resulting flake (c) are shown in Fig. 5. Although the [110], [200] and [220] peaks are still detectable, they show very poor crystallinity when compared with the ZIF-8 powder or the successful ZIF-8/6FDA–DAM:DABA(4:1) composite film. Furthermore, the [211], [310] and [222] peaks are completely undetectable in the flakes of the gelled dope. It is likely that the pendant carboxylic acid functional group reacted with the imidazolate linkers to produce this poor crystallinity. Due to the fact that some crystallinity remains in the ZIF-8/6FDA–DAM:DABA(4:1) flakes suggests that the ZIF-8 surface is reacting — and subsequently cross-linking with the

pendant carboxylic acid group on 6FDA–DAM:DABA(4:1), while the “core” of the ZIF-8 particle likely remains crystalline.

3.2.2. Film characterization

DSC and TGA analysis on the 20 wt% ZIF-8/6FDA–DAM:DABA(4:1) film reveal a negligible difference in T_g between neat polymer and the mixed matrix film, while the TGA data reveal a lower decomposition temperature for the MMM of $\sim 425^\circ\text{C}$, likely as a result of the ZIF-8 decomposing (Figs. S2 and S3) [45]. ATR (Fig. S4) does not reveal any significant peak shifts in the region of characteristic absorption for carboxylic acids as a result of including the ZIF-8 into 6FDA–DAM:DABA(4:1).

3.2.2.1. SEM/TEM Images of mixed matrix films. SEM images of the 20 wt% ZIF-8/6FDA–DAM:DABA(4:1) mixed matrix membrane films reveal a fairly homogenous dispersion of the ZIF-8 crystals throughout the polymer matrix (Fig. 6a). Adhesion to the polymer matrix, at least under magnifications used in SEM, appears to be excellent. The ZIF-8 particles appear to be approximately 40–150 nm in diameter, with the majority of particles being approximately 50 nm from SEM inspection. TEM images of the microtomed ZIF-8/6FDA–DAM:DABA(4:1) mixed matrix membranes reveal that the majority of the ZIF-8 particles had good adhesion to the polymer matrix (Fig. 6c and d). However, a minor portion of the dispersed ZIF-8 showed agglomerates of crystals (Fig. 6b). These non-ideal regions within the mixed matrix membrane will lead to higher yet non-selective fluxes and may also have small enough interparticle pores that high water activities will result in capillary condensation between the particles.

3.2.2.2. Water sorption isotherms. The primary motivation for using ZIF-8 as a permeability-enhancing filler is its adhesion to the polymer, its high flux, and its hydrophobicity. However, if the

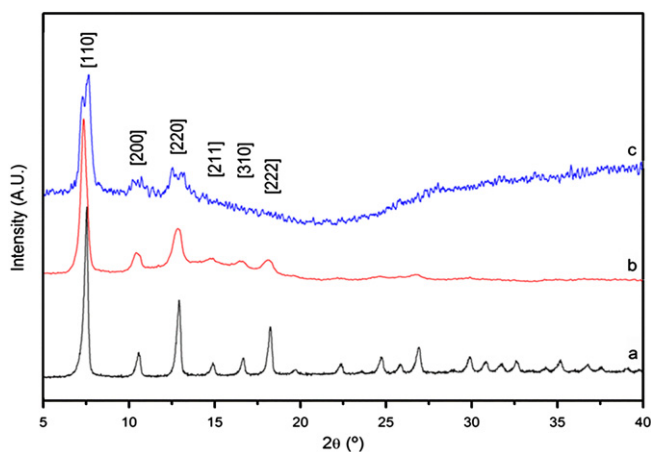


Fig. 5. Powder X-ray diffraction patterns for (a) ZIF-8 powder, (b) 20 wt% ZIF-8/6FDA–DAM:DABA(4:1) films made without sonication, and (c) flakes of 20 wt% ZIF-8/6FDA–DAM:DABA(4:1) after sonication.

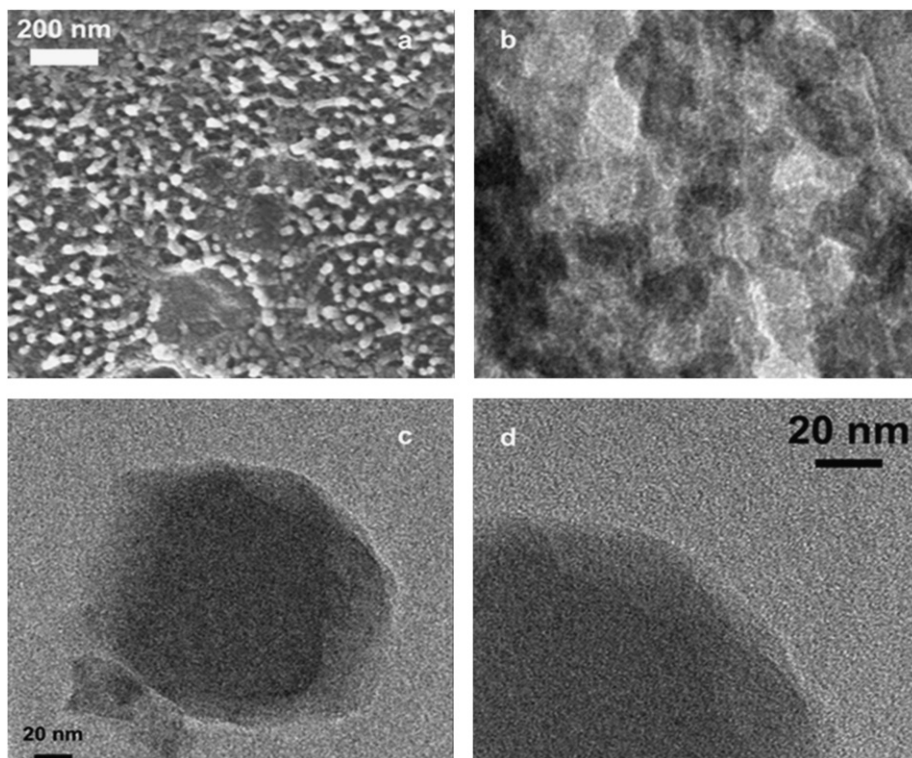


Fig. 6. Representative SEM (a) and HRTEM (b–d) micrographs of 20 wt% ZIF-8/6FDA–DAM:DABA(4:1) films. (b) Small domains of aggregates were found, while (c and d) show the adhesion and dispersion of the majority of the ZIF-8 particles (dark grey) within the 6FDA–DAM:DABA(4:1) matrix (light grey).

small portion of aggregates found in the ZIF-8/6FDA–DAM:DABA (4:1) have water condensed in the interparticle pores, then some of the advantage of including ZIF-8 will be undone. Water vapor sorption isotherms from 5% RH to 95% RH (Fig. 7) indicate that the ZIF-8 itself is quite hydrophobic, as expected. Furthermore, there is no discernible difference between the neat 6FDA–DAM:DABA (4:1) and the 20 wt% ZIF-8/6FDA–DAM:DABA(4:1) water isotherms. These experiments confirm that the small portion of undesirable ZIF-8 aggregates in the mixed matrix membrane do not deleteriously affect the membrane properties from a water condensation perspective.

3.2.3. CO₂/N₂ permeation results

Pure gas permeation on the 20 wt% ZIF-8/6FDA–DAM:DABA(4:1) reveals a marked CO₂ permeability enhancement with only marginal loss in CO₂/N₂ selectivity. The Robeson-style plot in Fig. 8 [35] shows the mixed matrix membrane has a CO₂ permeability of 553 ± 3 Barrers at 30 °C, which is a 2.5x increase in permeability over the neat 6FDA–DAM:DABA(4:1). Recent work has shown that ZIF-8 has a matrix-dependent permeability [24,25,45–51] and selectivity [52], and a CO₂/N₂ permselectivity of approximately 10 has been estimated recently in similar polymer matrices [52]. Thus, since as ZIF-8 has a modest

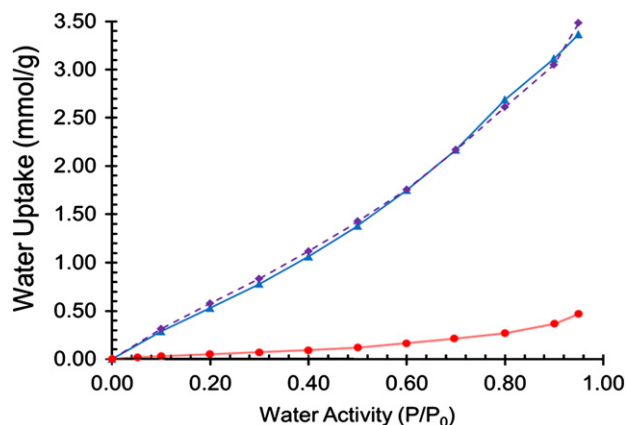


Fig. 7. Water sorption isotherms on ZIF-8 powder (red circles), neat 6FDA–DAM:DABA(4:1) films (blue triangles), and 20 wt% ZIF-8/6FDA–DAM:DABA(4:1) mixed matrix membrane films (purple diamonds). (For interpretation of the references to color in this figure legend, the reader is referred to the web version of this article.)

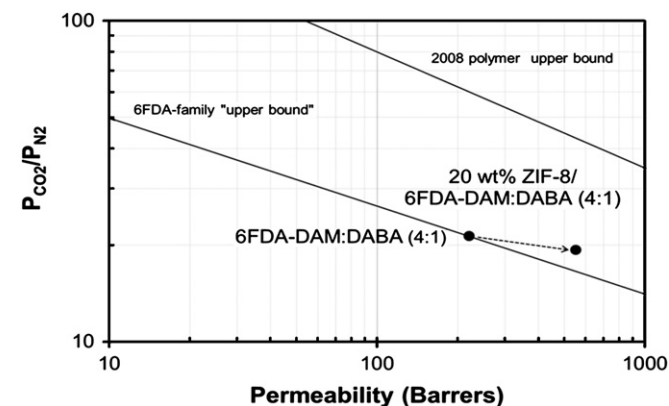


Fig. 8. Robeson plot [35] illustrating the effect of 20 wt% ZIF-8 addition to 6FDA–DAM:DABA(4:1) and a hypothetical 6FDA-family upper bound.

CO₂/N₂ selectivity, the resulting mixed matrix membrane has an ideal CO₂/N₂ permselectivity of 19.3 ± 0.3 ; a 9.3% decrease in selectivity relative to the neat film. Thus, when taken with the SEM/HRTEM images and water vapor isotherms (which indicate good adhesion between the ZIF and the polymer), it appears that the loss in selectivity is a result of the intrinsic properties of the ZIF-8, rather than poor adhesion between the polymer and the filler. As flux through the membrane has been shown to be the main way to decrease the overall CO₂ capture cost, the 2.5x increase in permeability more than offsets the 9.3% loss in permselectivity. This “proof-of-concept” scoping study highlights some potential paths forward for post-combustion CO₂ capture using hollow fiber membranes. If ZIF-8/polymer hollow fiber membranes are made (which have been previously demonstrated using Ultem[®] as the polymer matrix [25]) using 6FDA-based polymers, the resulting ultra-high flux fibers could drastically reduce CO₂ capture costs. For instance, if skin layer thicknesses could be reduced to 100 nm, a 20 wt% ZIF-8/6FDA–DAM:DABA(4:1) hollow fiber (utilizing 20 nm ZIF-8 particles [52]) could be expected to have wet CO₂ permeances of approximately 2000 GPU and a CO₂/N₂ permselectivity of approximately 19.5.

3.3. Process design

Preliminary process design calculations were performed using a custom-built cross-flow membrane model module [53] in Aspen Plus[®] to determine the cost of the CO₂ capture process using 6FDA–DAM:DABA(4:1) in its current form (neat polymer hollow fiber membranes). The model description can be found in the Supplementary material. We have also analyzed the effect of membrane permeance and CO₂/N₂ permselectivity on the overall membrane performance using three other cases. These cases include: (i) neat polymer hollow fibers with 100 nm skin thicknesses, (ii) 20 wt% ZIF-8/6FDA–DAM:DABA(4:1) hollow fibers with 150 nm skin layers, and (iii) 20 wt% ZIF-8/6FDA–DAM:DABA(4:1) with 100 nm skin layers. The process configuration considered here is the two-step counter-flow/sweep membrane process first proposed by Merkel et al. [10,11]. This configuration has many advantages over two-vacuum, two-stage processes; namely, the air sweep used in the second membrane effectively handles a portion of the separation for “free.” Furthermore, by using a condenser/compressor to treat the permeate of membrane I (Fig. 9), the challenging requirement of creating the required 95 mol% purity via membranes is removed.

The process modeling used the following assumptions for the CO₂ capture system. Compression equipment capital was assumed to cost \$500/kW, while the plant mill rate was assumed to be \$0.04/kWh. A capital installation factor of 1.6 was used and a plant capacity factor of 85% was assumed. CO₂ capture rates of 90% were used, and the CO₂ product purity was set to be greater than 95%. A feed pressure of 1.1 bar to the first membrane was used along with a permeate pressure of 0.2 bar in order to achieve a pressure ratio of 5.5 across the membrane. One hundred percent of the boiler feed air was assumed to contact membrane II. More than 95% of the water in the feed flue gas was assumed to permeate through the first membrane, which is a worst-case scenario due to the increased duty of the water condenser. Finally, the loss of efficiency in the boiler due to lower O₂ concentrations was neglected in order to make meaningful comparisons with previous work, which used the same assumption [10]. Recent work by MTR has given some support to this assumption [54].

As shown in Table 5, we benchmarked the model using spiral-wound membranes with a 1000 GPU CO₂ permeance and a CO₂/N₂ permselectivity of 50 as a base case [10]. Using a skidded cost of \$50/m² for spiral wound membranes in plastic modules,

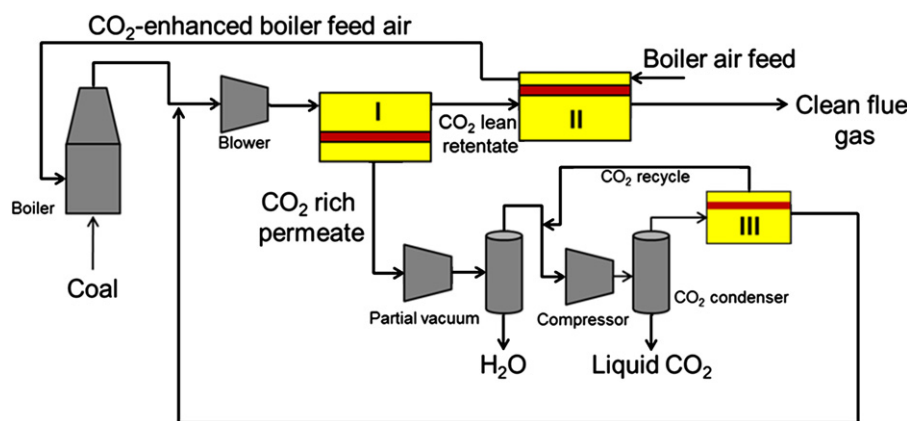


Fig. 9. Two-step counter-flow/sweep process arrangement. Membranes I and III operate in cross-flow mode, while membrane II operates in counter-flow/sweep mode. Adapted from [10].

Table 5

Comparison of membrane materials and morphologies for CO₂ capture using a two-step counter-flow/sweep membrane process for a 600 MW_e coal-fired power plant.

Case	(P/l) _{CO₂} (GPU)	CO ₂ /N ₂ Permselectivity	Membrane area (10 ⁶ m ²)	Plant electric derate (MW _e)
1. Base case (spiral wound)	1000	50	0.973	114.0
2. 6FDA–DAM:DABA(4:1) 415 nm skins	243	19.75	3.391	142.6
3. 6FDA–DAM:DABA(4:1) 100 nm skins	1000	19.75	1.070	145.0
4. 20 wt% ZIF-8/6FDA–DAM:DABA(4:1) 150 nm skins	1600	19.75	0.537	144.4
5. 20 wt% ZIF-8/6FDA–DAM:DABA(4:1) 100 nm skins	2000	19.75	0.430	145.3

and similar assumptions to Merkel et al., the membrane model yields surface areas and CO₂ capture costs consistent with those previously reported [10]. While spiral wound modules for high-pressure gas separations are typically \$500/m² [21] when delivered on a skid, Merkel et al. reasonably argue that skidded costs of \$50/m² for spiral-wound modules in plastic housing can be achieved. Hollow fiber membrane modules for high-pressure gas separations can be produced at a cost of \$20/m² [55], and by following similar trends for spiral-wound modules, have approximately \$100/m² skidded costs. However, due to the low-pressure operation planned for post-combustion CO₂ capture, much of the complexity of a membrane skid can be removed, and plastic housings are permissible. As such, we expect that hollow fiber membrane modules on a skid can be delivered for approximately \$10–\$20/m²; we used \$20/m² in this analysis. Due to the costs of a specialty polymer such as 6FDA–DAM:DABA(4:1), this low cost can likely be achieved given sufficient economies of scale (massive scales will be required for CO₂ capture). Moreover, dual-layer asymmetric hollow fiber spinning can be used [29], wherein a small amount of specialty polymer is co-spun with a low-cost support, thus making the cost estimates quite reasonable. Table 5 shows the total membrane surface area required for defect-free 6FDA–DAM:DABA(4:1) hollow fiber membranes using performance properties achieved in this study (243 GPU wet CO₂ permeance and wet CO₂/N₂ permselectivity of 19.75). We estimate that approximately 3.4 MM m² of membrane surface area is required due to the lower fluxes of the glassy hollow fiber membranes relative to the rubbery spiral wound membranes. Furthermore, the parasitic load (plant electric derate divided by the plant's nameplate capacity, Fig. 10a) was found to increase by 5.2 percentage points (a 25.2% increase) due to the lower selectivity of the hollow fiber membranes. However, as shown in Fig. 10b, the total number of 8" diameter modules required for the hollow fiber membrane system is approximately 13,070 (assuming 8000 m²/m³ packing), whereas the number of modules required for the base case spiral-wound system is approximately 50,000 modules (assuming 600 m²/m³ packing). In terms of

modules alone (compression systems, piping, fans, etc. not included), the total footprint required — assuming the modules are laid horizontally and stacked 10 high — is 1016 m² for the base case system, and 265 m² for the current 6FDA–DAM:DABA(4:1) hollow fiber membrane system. Finally, the CO₂ capture cost is approximately \$26.7/ton of CO₂ for the hollow fiber membrane system, while we estimate a cost of \$21.0/ton of CO₂ for the base case spiral-wound membranes (Fig. 10c).

Continued research most certainly can reduce the skin layer thickness of the 6FDA–DAM:DABA(4:1) towards 100–200 nm and could lead to the inclusion of flux-enhancing ZIF-8 particles in the fiber skin layer. These “advanced” cases (Table 5) show significant reductions in total membrane surface area required due to the higher fluxes of the advanced hollow fibers; however, similar parasitic loads are expected due to the selectivity of the material (Fig. 10a). Nonetheless, the total number of modules is reduced significantly to approximately 1656 modules (Fig. 10b), or a total footprint of 33 m² using the same assumptions as above. This possible order-of-magnitude reduction in system footprint is accompanied by competitive CO₂ capture costs of approximately \$23.1/ton of CO₂ (Fig. 10c).

4. Conclusions

Due to the overwhelming scale of CO₂ emissions from coal-fired power plants, any discussion of post-combustion CO₂ capture must first begin with the scalability of the CO₂ capture solution. Here, we propose highly scalable glassy polyimide hollow fiber membranes as an attractive option for post-combustion CO₂ capture. 6FDA–DAM:DABA(4:1) was synthesized and spun as a hollow fiber membrane. CO₂ permeances of 520 ± 9 GPU were obtained at 30 °C with a CO₂/N₂ permselectivity of 23.5. The defect-free hollow fibers had an apparent skin thickness of 415 ± 10 nm. Mixed gas and wet gas experiments showed a factor of 2 reduction in CO₂ permeance at 30 °C, while temperatures over 40 °C showed loss in selectivities. This likely

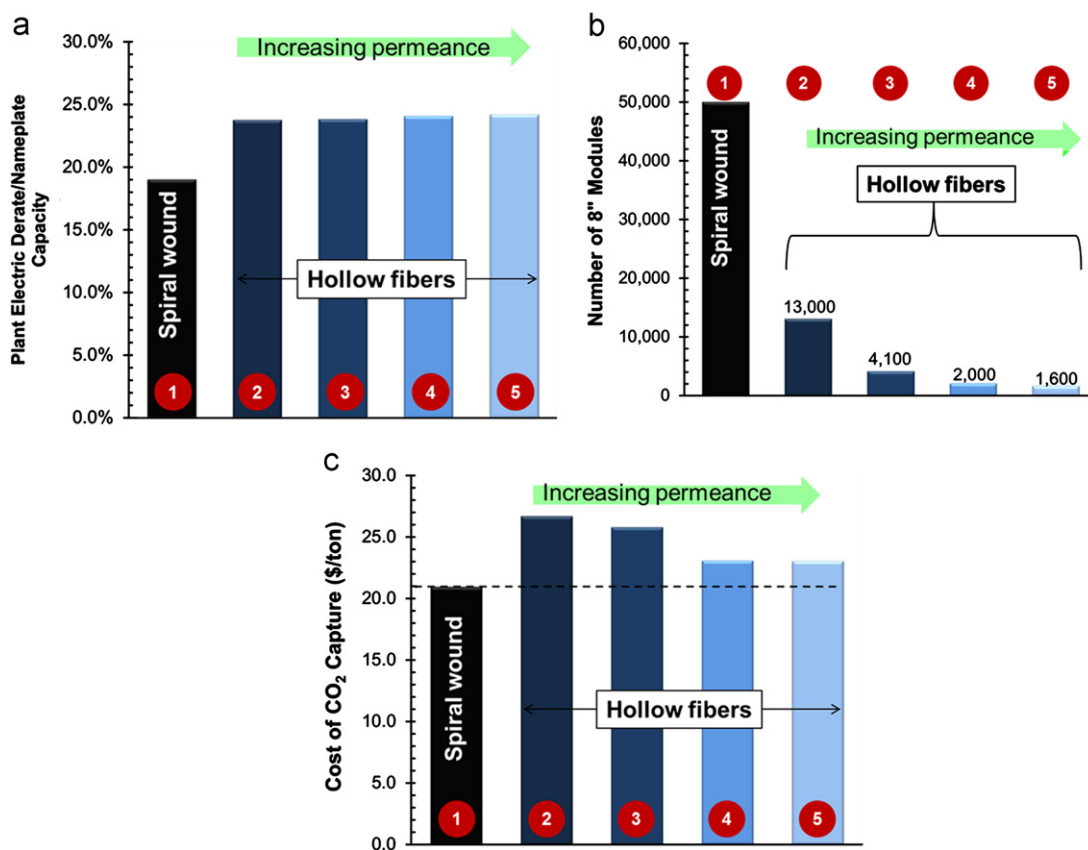


Fig. 10. Comparative process analysis results for 6FDA–DAM:DABA(4:1) hollow fiber membranes and control case in the counter-flow sweep arrangement. Red numbers on figure refer to specific cases listed in Table 5. (a) Parasitic load estimates, (b) number of 8' module elements estimate, and (c) cost of CO₂ capture. (For interpretation of the references to color in this figure legend, the reader is referred to the web version of this article.)

indicates the optimum temperature range for 6FDA–DAM:DABA (4:1) operation exists between 30 °C and 40 °C. Nonetheless, even in wet gas feeds, high CO₂ permeances (243.2 ± 2.2 GPU) were obtained. ZIF-8, a commercially available metal-organic framework from BASF, was used to improve the permeability of 6FDA–DAM:DABA(4:1) films. At 20 wt% loading, the membrane permeability increased by 250% over the neat polymer membrane, with only a modest 9.4% loss in CO₂/N₂ permselectivity. A process analysis using a two-step counter-flow/sweep membrane arrangement predicted power plant parasitic loads of approximately 24% for the 6FDA–DAM:DABA(4:1) hollow fiber membranes and CO₂ capture costs ranging from \$26.7/ton to \$23.1/ton, depending on the skin thickness of the membrane. These numbers are competitive with the current state-of-the-art spiral wound membranes [10], yet the analysis here predicts a 5–50x reduction in total modules required as a result of the hollow fiber morphology.

Finally, post-combustion CO₂ capture presents many challenges that must be addressed for effective worldwide deployment. Materials research needs include membrane stability to flue gas contaminants, oxygen, particulates and overall lifetime. Indeed, pilot-scale tests using hollow fiber membranes for flue gas dehydration have illustrated the challenges of a typical flue gas feed [56]. Process research needs encompass the materials research needs, but also requires an understanding of the effect of reduced oxygen on the boiler efficiency as well as the feasibility of ultra-large vacuum and compression equipment. From a scale-up perspective, hollow fibers have the potential to be produced in the quantities required for a worldwide deployment of post-combustion CO₂ capture systems. Based on our analysis here, 13 trillion meters of hollow fiber membrane are required to capture

90% of the CO₂ emitted from over 3250 coal-fired power plants worldwide. To put this into perspective, the synthetic textile industry produces approximately 470 trillion meters of fiber per year [57]. Furthermore, while ZIF-8 production is still at the pilot scale (~ 0.04 kton/yr [56]), if ZIF-8 is to only be included in the thin skin layers of composite hollow fibers [29], we estimate that approximately 16,800 t of ZIF-8 will be required, or approximately 5.6 kton/yr assuming a 3 year fiber lifetime [58]. The materials and process work performed here, along with these simple estimates of production rates and capacity highlight the potential for a hollow fiber membrane platform for post-combustion CO₂ capture.

Acknowledgments

W.J. Koros thanks Award no. KUS-I1-011-21 made by the King Abdullah University of Science and Technology (KAUST) for financial support.

Appendix A. Supporting information

Supplementary data associated with this article can be found in the online version at <http://dx.doi.org/10.1016/j.memsci.2012.08.026>.

References

- [1] Annual Energy Outlook 2012, Energy Information Administration, Report no. DOE/EIA-0383ER, 2012.

- [2] CO₂ Emissions from Fuel Combustion, International Energy Agency, 2011.
- [3] CCS Retrofit: Analysis of the Globally Installed Coal-Fired Power Plant Fleet, International Energy Agency, 2012.
- [4] Annual Coal Report 2012, Energy Information Administration, Report no. DOE/EIA-0584, 2012.
- [5] Natural Gas Processing Plants in the United States: 2010 Update, Energy Information Administration, 2012.
- [6] E. Favre, Carbon dioxide recovery from post-combustion processes: can gas permeation membranes compete with absorption? *J. Membr. Sci.* 294 (2007) 50–59.
- [7] L. Zhao, E. Rienecke, L. Blum, D. Stolten, Multi-stage gas separation membrane processes used in post-combustion capture: Energetic and economic analyses, *J. Membr. Sci.* 359 (2010) 160–172.
- [8] L. Zhao, R. Menzer, E. Rienecke, L. Blum, D. Stolten, Concepts and investment cost analyses of multi-stage membrane systems used in post-combustion processes, *Energy Proc.* 1 (2009) 269–278.
- [9] M.H.M. Chowdhury, X. Feng, P. Douglas, E. Croiset, A new numerical approach for a detailed multicomponent gas separation membrane model and AspenPlus simulation, *Chem. Eng. Technol.* 28 (2005) 773–782.
- [10] T.C. Merkel, H. Lin, X. Wei, R. Baker, Power plant post-combustion carbon dioxide capture: an opportunity for membranes, *J. Membr. Sci.* 359 (2010) 126–139.
- [11] R.W. Baker, J.G. Wijmans, T.C. Merkel, H. Lin, R. Daniels, S. Thompson, Gas Separation Process Using Membranes with Permeate Sweep to Remove CO₂ from Combustion Gases, Patent no. PCT/US2009/002874, 2009.
- [12] Current and Future Technologies for Power Generation with Post-Combustion CO₂ Capture, National Energy Technology Lab, Report no. DOE/EIA-2012/1557, 2012.
- [13] U. Senthilkumar, B.S.R. Reddy, Polysiloxanes with pendent bulky groups having amino-hydroxy functionality: structure–permeability correlation, *J. Membr. Sci.* 292 (2007) 72–79.
- [14] H. Lin, B.D. Freeman, Gas solubility, diffusivity and permeability in poly(ethylene oxide), *J. Membr. Sci.* 239 (2004) 105–117.
- [15] K.-I. Okamoto, N. Umeo, S. Okamoto, K. Tanaka, H. Kita, Selective permeation of carbon dioxide over nitrogen through polyethyleneoxide-containing polyimide membranes, *Chem. Lett.* 22 (1993) 225–228.
- [16] C.J. Orme, M.K. Harrup, T.A. Luther, R.P. Lash, K.S. Houston, D.H. Weinkauff, F.F. Stewart, Characterization of gas transport in selected rubbery amorphous polyphosphazene membranes, *J. Membr. Sci.* 186 (2001) 249–256.
- [17] T.-S. Chung, W.H. Lin, R.H. Vora, The effect of shear rates on gas separation performance of 6FDA-durene polyimide hollow fibers, *J. Membr. Sci.* 167 (2000) 55–66.
- [18] I.C. Omole, R.T. Adams, S.J. Miller, W.J. Koros, Effects of CO₂ on a high performance hollow-fiber membrane for natural gas purification, *Ind. Eng. Chem. Res.* 49 (2010) 4887–4896.
- [19] C.-C. Chen, W. Qiu, S.J. Miller, W.J. Koros, Plasticization-resistant hollow fiber membranes for CO₂/CH₄ separation based on a thermally crosslinkable polyimide, *J. Membr. Sci.* 382 (2011) 212–221.
- [20] H.F. Samuelson, Spinneret Assembly, US Patent 1989, Patent no. 4,861,661.
- [21] R.W. Baker, K. Lokhandwala, Natural gas processing with membranes: an overview, *Ind. Eng. Chem. Res.* 47 (2008) 2109–2121.
- [22] J.H. Kim, W.J. Koros, D.R. Paul, Effects of CO₂ exposure and physical aging on the gas permeability of thin 6FDA-based polyimide membranes, Part 2: with crosslinking, *J. Membr. Sci.* 282 (2006) 32–43.
- [23] W. Qiu, C.-C. Chen, L. Xu, W.J. Koros, Effects of polyimide chemical structure on membrane gas separation performance, in: Proceedings of the North American Membrane Society, Annual Meeting, New Orleans, LA, June 13 2012.
- [24] J.C.S. Remi, T. Rémy, V. Van Hunskerken, S. van de Perre, T. Duerinck, M. Maes, D. De Vos, E. Gobechiya, C.E.A. Kirschhock, G.V. Baron, J.F.M. Denayer, Biobutanol separation with the metal-organic framework ZIF-8, *ChemSusChem* 4 (2011) 1074–1077.
- [25] Y. Dai, J.R. Johnson, O. Karvan, D.S. Sholl, W.J. Koros, W.J. Ultem, ®/ZIF-8 mixed matrix hollow fiber membranes for CO₂/N₂ separations, *J. Membr. Sci.* 401–402 (2012) 76–82.
- [26] C. Zhang, Y. Dai, J.R. Johnson, O. Karvan, W.J. Koros, High performance ZIF-8/6FDA-DAM mixed matrix membrane for propylene/propane separations, *J. Membr. Sci.* 389 (2012) 34–42.
- [27] T. Moore, S. Damle, P. Williams, W.J. Koros, Characterization of low permeability gas separation membranes and barrier materials; design and operation considerations, *J. Membr. Sci.* 245 (2004) 227–231.
- [28] L.M. Costello, W.J. Koros, Thermally stable polyimide isomers for membrane-based gas separations at elevated temperatures, *J. Polym. Sci. B* 33 (1995) 135–146.
- [29] S. Husain, Mixed Matrix Dual Layer Hollow Fiber Membranes for Natural Gas Separation, Ph.D. Dissertation, Georgia Institute of Technology, Atlanta, GA, 2006.
- [30] D.W. Wallace, Crosslinked Hollow Fiber Membranes for Natural Gas Purification and their manufacture from novel polymers, Ph.D. Dissertation, in: Chemical Engineering, The University of Texas at Austin, Austin, TX, 2004.
- [31] C.M. Zimmerman, W.J. Koros, Polypyrrolones for membrane gas separations. II. Activation energies and heats of sorption, *J. Polym. Sci. B* 37 (1999) 1251–1265.
- [32] W.J. Koros, D.R. Paul, Design considerations for measurement of gas sorption in polymers by pressure decay, *J. Polym. Sci., Polym. Phys. Ed.* 14 (1976) 1903–1907.
- [33] R.P. Lively, J.A. Mysona, R.R. Chance, W.J. Koros, Formation of defect-free latex films on porous fiber supports, *ACS Appl. Mater. Interfaces* 3 (2011) 3568–3582.
- [34] S.B. Newman, E. Borysko, M. Swerdlow, New sectioning techniques for light and electron microscopy, *Science* 110 (1949) 66–68.
- [35] L.M. Robeson, The upper bound revisited, *J. Membr. Sci.* 320 (2008) 390–400.
- [36] W.J. Koros, M. Coleman, D. Walker, Controlled permeability polymer membranes, *Annu. Rev. Mater. Sci.* 22 (1992) 47–89.
- [37] A. Torrisi, C. Mellot-Draznieks, R.G. Bell, Impact of ligands on CO₂ adsorption in metal-organic frameworks: First principles study of the interaction of CO₂ with functionalized benzenes. II. Effect of polar and acidic substituents, *J. Chem. Phys.* 132 (2010) 044705.
- [38] S. Kiil, M.L. Michelsen, K. Dam-Johansen, Experimental investigation and modeling of a wet flue gas desulfurization pilot plant, *Ind. Eng. Chem. Res.* 37 (1998) 2792–2806.
- [39] J.-J. Qin, R. Wang, T.-S. Chung, Investigation of shear stress effect within a spinneret on flux, separation and thermomechanical properties of hollow fiber ultrafiltration membranes, *J. Membr. Sci.* 175 (2000) 197–213.
- [40] D.K. Yang, W.J. Koros, H.B. Hopfenberg, V.T. Stannett, Sorption and transport studies of water in kapton polyimide. I, *J. Appl. Polym. Sci.* 30 (1985) 1035–1047.
- [41] G.Q. Chen, C.A. Scholes, G.G. Qiao, S.E. Kentish, Water vapor permeation in polyimide membranes, *J. Membr. Sci.* 379 (2011) 479–487.
- [42] K.S. Park, Z. Ni, A.P. Côte, J.Y. Choi, R. Huang, F.J. Uribe-Romo, H.K. Chae, M. O’Keeffe, O.M. Yaghi, Exceptional chemical and thermal stability of zeolitic imidazolate frameworks, *Proc. Nat. Acad. Sci. USA* 103 (2006) 10186–10191.
- [43] J.A. Thompson, C.R. Blad, N.A. Brunelli, M.E. Lydon, R.P. Lively, C.W. Jones, S. Nair, Hybrid zeolitic imidazolate frameworks: controlling framework porosity and functionality by mixed-linker synthesis, *Chem. Mater.* 24 (2012) 1930–1936.
- [44] D. Fairen-Jimenez, S.A. Moggach, M.T. Wharmby, P.A. Wright, S. Parsons, T. Düren, Opening the gate: framework flexibility in ZIF-8 explored by experiments and simulations, *J. Am. Chem. Soc.* 133 (2011) 8900–8902.
- [45] X.-C. Huang, Y.-Y. Lin, J.-P. Zhang, X.-M. Chen, Ligand-directed strategy for zeolite-type metal-organic frameworks: zinc(II) imidazolates with unusual zeolitic topologies, *Angew. Chem. Int. Ed. Engl.* 45 (2006) 1557–1559.
- [46] J.A. Thompson, K.W. Chapman, W.J. Koros, C.W. Jones, S. Nair, Sonication-induced Ostwald ripening of ZIF-8 nanoparticles and formation of ZIF-8/polymer composite membranes, *Microporous Mesoporous Mater.* 158 (2012) 292–299.
- [47] M.J.C. Ordóñez, K.J. Balkus Jr., J.P. Ferraris, I.H. Musselman, Molecular sieving realized with ZIF-8/Matrimid® mixed-matrix membranes, *J. Membr. Sci.* 361 (2010) 28–37.
- [48] B. Zornoza, C. Tellez, J. Coronas, J. Gascon, F. Kapteijn, Metal organic framework based mixed matrix membranes: an increasingly important field of research with a large application potential, *Microporous Mesoporous Mater.*, in press <http://dx.doi.org/10.1016/j.micromeso.2012.03.012>.
- [49] W.J. Koros, R.P. Lively, J.A. Thompson, Y. Dai, J.-S. Lee, K. Zhang, C. Zhang, M.E. Dose, M. Bighane, C.W. Jones, S. Nair, J.R. Johnson, Metal-Organic Framework Matrix-Dependent Mass Transport Phenomena, ACS National Meeting, Philadelphia, PA, August 19th, 2012.
- [50] K. Diaz, M. Lopez-Gonzalez, L.F.d. Castillo, E. Riande, Effect of zeolitic imidazolate frameworks on the gas transport performance of ZIF8-poly(1,4-phenylene ether-ether-sulfone) hybrid membranes, *J. Membr. Sci.* 383 (2011) 206–213.
- [51] B. Zornoza, B. Seoane, J.M. Zamaro, C. Tellez, J. Coronas, Combination of MOFs and zeolites for mixed-matrix membranes, *ChemPhysChem* 12 (2011) 2781–2785.
- [52] C. Zhang, R.P. Lively, K. Zhang, J.R. Johnson, O. Karvan, W.J. Koros, Unexpected molecular sieving properties of zeolitic imidazolate framework 8, *J. Phys. Chem. Lett.* 3 (2012) 2130–2134.
- [53] Y. Shindo, T. Hakuta, H. Yoshitome, H. Inoue, Calculation methods for multicomponent gas separation by permeation, *Sep. Sci. Technol.* 20 (1985) 445–459.
- [54] K. Amo, Z. He, J. Kaschemekat, T. Merkel, M. Mohammed, S. Pande, X. Wei, S. White, Slipstream testing of a membrane CO₂ capture process. NETL CO₂ Capture Meeting, Pittsburgh, PA, July 9th, 2012.
- [55] D.Q. Vu, W.J. Koros, S.J. Miller, Mixed matrix membranes using carbon molecular sieves I. Preparation and experimental result, *J. Membr. Sci.* 211 (2003) 311–334.
- [56] H. Sijbesma, K. Nymeyer, R. van Marwijk, R. Heijboer, J. Potreck, M. Wessling, Flue gas dehydration using polymer membranes, *J. Membr. Sci.* 313 (2008) 263–276.
- [57] The Fiber Year 2009/2010: A World Survey on Textile and Nonwovens Industry, Oerlikon, vol. 10, 2010.
- [58] M. Jacoby, Heading to Market with MOFs, *Chem. Eng. News* 86 (34) (2008) 13–16.